Coherent Vorticity Holes from 2D Turbulence Decaying in a Background Shear Flow

X.-P. Huang, K. S. Fine, and C. F. Driscoll

*Physics Department and Institute for Pure and Applied Physical Sciences, University of California at San Diego,
La Jolla, California 92093*
(Received 3 November 1994)

Freely decaying 2D turbulence in magnetized electron columns has been measured using a phosphor screen/CCD camera diagnostic. The relaxation towards axisymmetric equilibrium is hindered by medium-sized coherent vorticity holes which persist for hundreds of column rotations despite the strong negative rotational shear. These holes tend to settle into symmetric configurations in the column, give a negative skew to the measured vorticity fluctuations, and are eventually destroyed due to a slow outward radial creep.

Coherent structures are important in the dynamics and transport of many flows. In two-dimensional (2D) freely decaying Navier-Stokes turbulence, computer simulations have demonstrated that self-coherent vortices emerge from random initial conditions and dominate the late-time relaxation [1]. Experiments using thin soap films and electrolyte have observed similar vortices, despite non-2D effects associated with the boundary layers and free surfaces [2,3]. Theoretical studies have analyzed coherent structures, such as drift-wave vortices, in various plasma systems [4,5]. Experimentally, the existence of such plasma structures is generally inferred from point probe measurements [6–9], and it is often presumed that these structures are destroyed by shear in the background flow. 2D quasigeostrophic models of sheared planetary atmospheres exhibit vortices [10,11], and computer simulations [11] and driven fluid experiments [12] have demonstrated the persistence of prograde vortices.

In this paper, we characterize freely decaying 2D turbulence in magnetized electron columns, and find that coherent density holes (i.e., prograde vortices) survive for hundreds of column rotations. An initially hollow column exhibits instabilities, transport, and fine-scale turbulence [13], then relaxes to an axisymmetric minimum enstrophy metaequilibrium with essentially no energy loss, the "selective decay" consistent with hypothesis [14]. Here, we show that this relaxation is slow because it is hindered by the longevity of elliptical density holes. The orientation and shape of these holes agree with an inviscid equilibrium model for vorticity patches in a background shear flow [15]. Hole interactions lead to a preferred configuration of two diametrically opposed holes on a distorted core (a "tripole"). On a time scale of hundreds of column bulk rotations, these holes creep radially outward and are eventually destroyed. Because of these coherent holes, the observed fluctuation relaxation rate is about 50 times slower than expected from simple passive tracer mixing, and the measured fluctuations are negatively skewed from Gaussian.

Figure 1 shows the experimental device with the imaging diagnostic. Electrons from a tungsten filament are trapped in a series of conducting cylinders (radius $R_w = 3.05$ cm) enclosed in a vacuum chamber ($\sim 10^{-9}$ torr). The electrons are contained axially by negative voltages (-150 V) on the two end cylinders, and confined radially by a uniform axial magnetic field ($B_z = 422$ G), resulting in a confinement time of about 1 s [13]. The trapped electron column typically has density $n \leq 1 \times 10^7$ cm^{-3}, radius $R_p \sim 1.5$ cm, and axial length $L_p \sim 50$ cm. The individual electrons have $kT \sim 1$ eV, giving an axial bounce time (~ 2 μs) much smaller than the column bulk rotation time (~ 10 μs), and a small gyroradius (~ 50 μm).

In the z-averaged $\mathbf{E} \times \mathbf{B}$ drift approximation [13], the (r, θ) flow of the electrons is described by the 2D drift Poisson equations,

$$\frac{\partial n}{\partial t} + \mathbf{v} \cdot \nabla n = 0, \ \mathbf{v} = -\frac{c}{B_z} \nabla \phi \times \hat{\mathbf{z}}, \ \nabla^2 \phi = 4\pi e n,$$

(1)

where $\mathbf{v}(r, \theta)$ is the drift velocity and $-e$ is the electron charge. The electron density $n(r, \theta)$ is proportional to the flow vorticity $\zeta(r, \theta)$, since $\zeta \equiv \hat{\mathbf{z}} \cdot (\nabla \times \mathbf{v}) = (4\pi e c/B_z)n$. The electrostatic potential $\phi(r, \theta)$ is proportional to the stream function, and the nonzero $\partial \phi / \partial r$ at the wall gives a true free-slip boundary condition. Equations (1) are isomorphic to the Euler equation that governs 2D inviscid incompressible fluids. For fine spatial scales or long times, plasma "viscous" or diffusive effects [16,17] not contained in Eqs. (1) are significant; however,
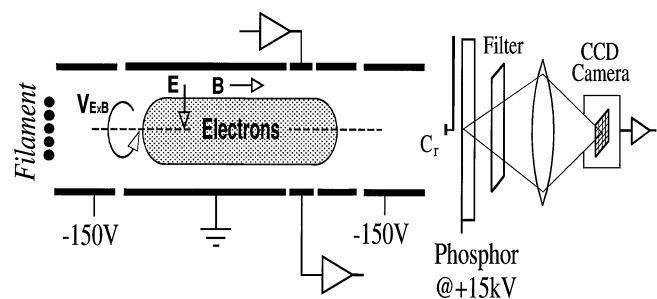

FIG. 1. The cylindrical experimental apparatus with phosphor screen/CCD camera diagnostic.

these are *not*, in general, modeled by the Navier-Stokes equation.

Experimentally, we first trap a stable quiescent column, then hollow it [13] and follow the instabilities and relaxation. At any time t, we dump the column axially onto a 3.2 cm phosphor screen biased to 15 kV. The fluorescence, proportional to the z-integrated electron density, is imaged by a low-noise charge-coupled device (CCD) camera with pixel area of $(130 \ \mu m)^2$ on the screen. Also, a mobile charge collector C_r gives independent density measurements at any r. The time evolution is obtained by observing many columns with essentially identical initial conditions.

Images of the electron density $n(r, \theta, t)$ (i.e., vorticity ζ) at 6 times during the evolution are displayed as false-color contour plots in Fig. 2. The initial hollow column is seeded with a slight $m = 2$ (i.e., $\cos 2\theta$) perturbation [13], and by $t = 3\tau_R$ the unstable $m = 2$ mode is near nonlinear saturation. Here, $\tau_R \equiv 10 \ \mu s$ is the "large eddy" turnover time. The evolution during the next $(20-30)\tau_R$ involves vortex merger, density filamentation, strong turbulent mixing, and fine-scale dissipation, resulting in transport to a stable vorticity profile with decaying fluctuations [13,18]. As is seen in the images at $40\tau_R$ and $100\tau_R$, long-lived self-coherent holes dominate the late-time fluctuations, slowing down the relaxation towards a fully axisymmetric metaequilibrium.

Figure 3 shows the θ averaged radial profiles of vorticity, $\langle\zeta\rangle$, angular velocity ω_R, and angular velocity shear $r d\omega_R/dr$ obtained from the measured $n(r, \theta)$ at $t = 100\tau_R$. Note that lower case r is scaled as $r \equiv R/R_w$, where R is in cm. The angular velocity is calculated from the measured images, as $\omega_R(r) = \int_0^r dr' \, r' \langle\zeta\rangle/r^2$. By $100\tau_R$, the column is globally stable, since both $\langle\zeta\rangle$ and ω_R are monotonically decreasing with radius. The

ω_R profile at $t = 100\tau_R$ is representative of the mean rotation during the relaxation, since it varies less than 10% during the period $40 \leq t/\tau_R \leq 10^5$.

The longevity of the vorticity holes in the images of Fig. 2 suggests that the holes can be regarded as negative vortices in equilibrium with the background shear flow. The inviscid equilibria of uniform vorticity patches in an imposed background flow are ellipses, as first derived by Moore and Saffman [15]. In our case, the mean background flow is purely rotational, i.e., $\langle\mathbf{v}\rangle = \omega_R(r) r \hat{\boldsymbol{\theta}}$, leading to a simple linear shear in the vicinity of any point. Therefore, the equilibrium depends only on the scaled shear

$$\sigma \equiv r_v \frac{d\omega_R}{dr}\Big|_{r_v} \Big/ \Delta\zeta_v,$$

where $\Delta\zeta_v$ is the difference between the vorticity at the center of the vortex (at radius r_v) and the background vorticity $\langle\zeta\rangle$ at r_v. Since the rotational shear considered here is everywhere negative, the equilibria are ellipses oriented along $\hat{\boldsymbol{\theta}}$ (for holes with $\sigma > 0$) or along $\hat{\mathbf{r}}$ (for clumps with $\sigma < 0$) [15].

Figure 4 shows the predicted and measured hole aspect ratios $\lambda \equiv a/b$, where a and b are the elliptical axes along θ and r directions, respectively. Here, λ and σ are measured directly from 16 images at times $40 \leq t/\tau_R \leq 400$. Reasonable agreement between the measurement and the model is found, validating the applicability of the model to individual holes in this system. (Of course, the actual holes have finite size and nonuniform interior vorticity distribution, and neither the deformation of the background flow nor the influence of other holes is included in this simple model.) The holes are robust because they are prograde with respect to the negative background shear, whereas clumps would be retrograde.
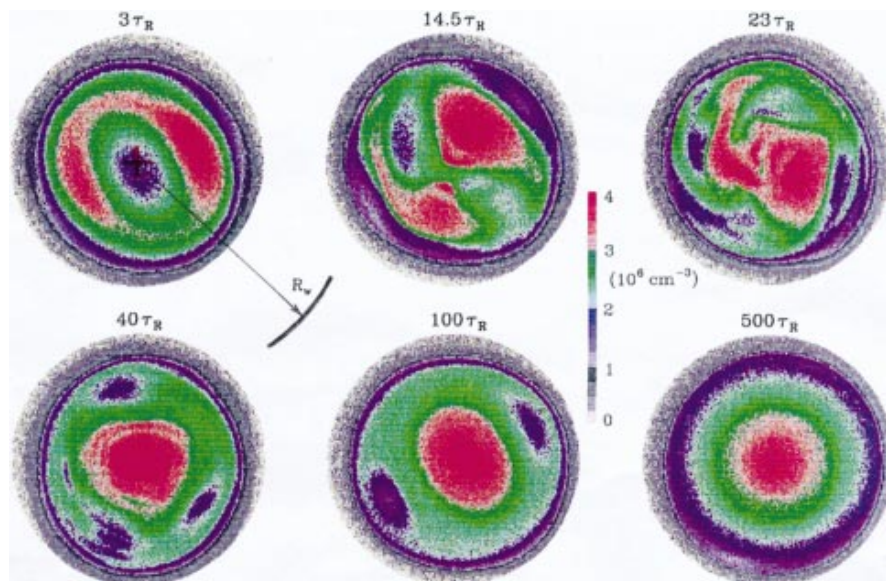

FIG. 2.   False-color camera images of electron density (i.e., vorticity) showing the evolution of an initially hollow electron column.
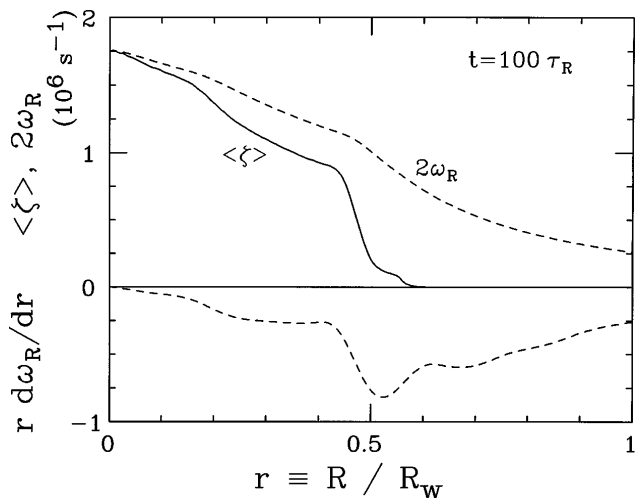
FIG. 3. Radial profiles of the θ averaged vorticity $\langle \zeta \rangle$, rotation ω_R, and shear $r\, d\omega_R/dr$.

In the model, holes of any depth $\Delta \zeta_h$ can survive in the background flow with negative shear. Of course, a shallow hole would be very elongated, and the local model is no longer valid. In contrast, a clump must have relative vorticity

$$\Delta \zeta_c \geq (3 + 2\sqrt{2})\, r_c \left| \frac{d\omega_R}{dr} \right|_{r_c} \qquad (2)$$

to be in equilibrium. Such very intense clumps are not observed for evolutions from initially smooth distributions such as Fig. 2. If we approximate the background as $\langle \zeta \rangle = \zeta_0 [1 - (r/r_0)^2]$, then $\Delta \zeta_c$ cannot be large enough to satisfy Eq. (2) provided the clump vorticity is no greater than the central vorticity (i.e., $\zeta_c \leq \zeta_0$). However, long-lived clumps *have* been observed in this apparatus during evolutions of highly filamented initial conditions with low shear profiles, apparently satisfying the condition of Eq. (2) [19]. Also, a similar limit to vortex stability has recently been measured in a system with a controlled background shear [20].
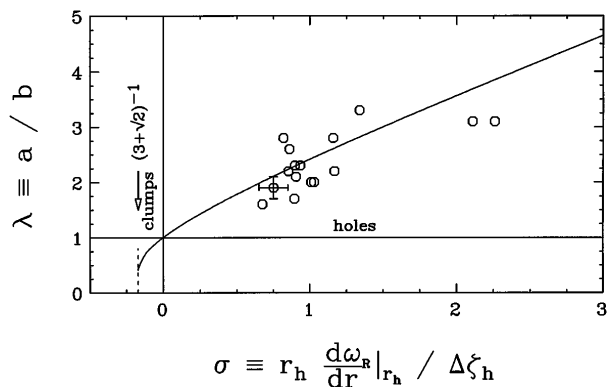
After about $40\tau_R$, the number of observed holes decreases with time, and the remaining holes tend to organize into symmetric configurations. After $80\tau_R$, virtually all the images are in the tripolar configuration of a deformed central core and two elliptical holes opposite in θ, typified by Fig. 2 at $100\tau_R$. The decrease in the number of holes with time is apparently due to mutual advection and merger of the holes [11]. These merger events have been observed in a few camera images, but the shot-to-shot irreproducibility precludes imaging the dynamics. The tripole state is stable for hundreds of τ_R because of hole-induced distortion of the background flow: The elongated core in Fig. 2 at $100\tau_R$ maintains the θ positions of the two holes.

In these evolutions, the quasistable tripolar configuration is eventually destroyed by a slow outward creep of the holes. Figure 5 shows the radial position r_h of the hole centers versus time, measured from the images with tripolar configuration: The holes move from $r_h \simeq 0.35$ to $r_h \simeq 0.50$ in about $500\tau_R$. Scattering of the data points reflects the shot-to-shot irreproducibility of the evolutions. The cause of this outward motion is unknown at present. However, experiments varying L_p and B_z suggest that this outward creep is a 2D $\mathbf{E} \times \mathbf{B}$ drift effect [18]. When the holes approach the edge of the column (at $r \simeq 0.57$), they apparently filament in the θ direction and are destroyed.

These long-lived coherent holes cause the measured shot-to-shot density fluctuations to decay much slower than expected from a naive passive tracer model. This model postulates that all fluctuations are just being distorted and filamented by the background shear [21], and then averaged over (coarse-grained) by the charge collector C_r [18]. This gives a relaxation of the measured fluctuation level as

$$\tilde{n}(r, t_0 + \Delta t) = \tilde{n}(r, t_0)\, 2 J_1(\chi_m\, \Delta t)/(\chi_m\, \Delta t), \qquad (3)$$

where $\chi_m(r) = -(m d_c/2)\, d\omega_R/dr$, $d_c = 0.13$ is the scaled diameter of the collector, and m characterizes the decaying perturbation as $\cos(m\theta)$. Figure 6 shows the rms variation $\tilde{n}$ in the charge collected on C_r at $r = 0.33$,

FIG. 4. Measured hole aspect ratio λ vs normalized background shear σ and Moore-Saffman model (curve).
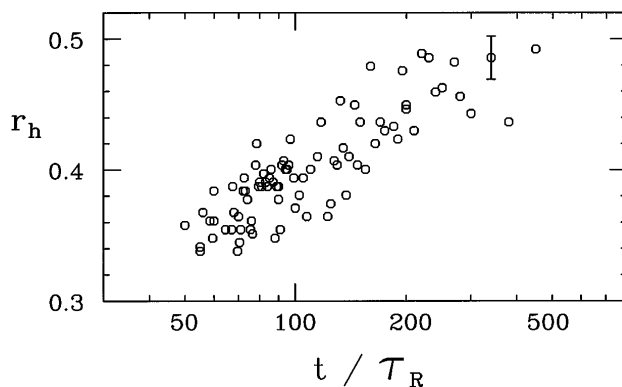

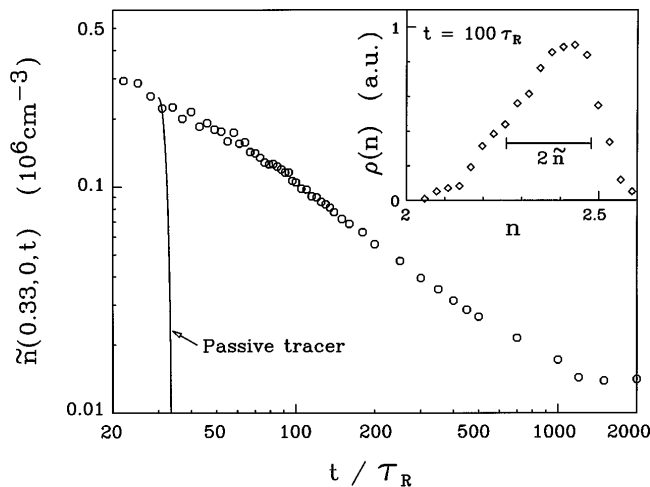FIG. 5. Radial positions of symmetric two-hole configurations versus time.

FIG. 6. Measured fluctuation level $\tilde{n}$ vs time, and predicted passive tracer mixing. The inset shows the PDF $\rho(n)$.

$\theta = 0$, from 1000 nominally identical evolutions at each time t. After growing during the initial instability period, $\tilde{n}$ relaxes with a time scale of $(100–200)\tau_R$. For $m = 2$, the passive tracer relaxation is shown as the solid curve, with an e-folding decay time $\simeq 3\tau_R$ determined from the shear profile of Fig. 3. The measured fluctuation decay rate is over 50 times slower than the passive tracer mixing.

The holes also produce a skewed non-Gaussian probability distribution function (PDF) for the density measurements. The inset in Fig. 6 shows the measured PDF of density $n(0.33, 0)$ at $t = 100\tau_R$. The localized density holes such as the ones shown in Fig. 2 give a skew at low densities, reflecting the probability that they are at the same (r, θ) as the collector C_r at the time of the measurement.

The measured fluctuations $\tilde{n}$ can also reflect shot-to-shot variations in the axisymmetric radial profile, or azimuthal distortion modes (Kelvin modes). The measured time-asymptotic radial profile variations ($\tilde{n} \sim 10^4$ cm^{-3}) reflect either incomplete relaxation to the 2D metaequilibrium or sensitivity to small shot-to-shot perturbations in the initial circulation, angular momentum, and energy [14]. Globally coherent Kelvin modes varying as $\delta n_m(r)\cos(m\theta)$ are damped if there is a linear or nonlinear resonance between the mode and background rotation [22].

Finally, we note that these prograde self-coherent vortices may be prevalent inside long-lived large vortices in more complex flows, such as the freely decaying Navier-Stokes turbulence [1]. Of course, the spatial scales of these vortices must be larger than the dissipation scale or they would be destroyed by viscosity. Furthermore, prograde drift-wave vortices may be able to survive in the edge layers of various plasma devices despite the shear of the mean flows in these regions.

[1] J. C. McWilliams, J. Fluid Mech. **146**, 21 (1984); R. Benzi *et al.*, Europhys. Lett. **3**, 811 (1987); A. Babiano *et al.*, J. Fluid Mech. **183**, 379 (1987); W. H. Matthaeus *et al.*, Phys. Rev. Lett. **66**, 2731 (1991); G. F. Carnevale *et al.*, *ibid.* **66**, 2735 (1991).
[2] M. Gharib and P. Derango, Physica (Amsterdam) **37D**, 406 (1989).
[3] P. Tabeling *et al.*, Phys. Rev. Lett. **66**, 2772 (1991).
[4] W. Horton *et al.*, Phys. Fluids **29**, 1004 (1986); X. N. Su *et al.*, Phys. Fluids B **3**, 921 (1991).
[5] A. E. Koniges, J. A. Crotinger, and P. H. Diamond, Phys. Fluids B **4**, 2785 (1992).
[6] S. J. Zweben, Phys. Fluids **28**, 974 (1985).
[7] T. Huld *et al.*, Phys. Fluids B **3**, 1609 (1991).
[8] H. Y. W. Tsui *et al.*, Phys. Rev. Lett. **70**, 2565 (1993).
[9] P. Tham and A. K. Sen, Phys. Rev. Lett. **72**, 1020 (1994).
[10] E. J. Hopfinger and G. J. F. van Heijst, Annu. Rev. Fluid Mech. **25**, 241 (1993).
[11] P. S. Marcus, Nature (London) **331**, 693 (1988); P. S. Marcus, Annu. Rev. Astron. Astrophys. **31**, 523 (1993).
[12] J. Sommeria, S. D. Meyers, and H. L. Swinney, Nature (London) **331**, 689 (1988).
[13] *Non-Neutral Plasma Physics,* edited by C. W. Roberson and C. F. Driscoll, AIP Conf. Proc. No. 175 (AIP, New York, 1988); C. F. Driscoll and K. S. Fine, Phys. Fluids B **2**, 1359 (1990).
[14] X.-P. Huang and C. F. Driscoll, Phys. Rev. Lett. **72**, 2187 (1994).
[15] D. W. Moore and P. G. Saffman, in *Aircraft Wake Turbulence and its Detection* (Plenum, New York, 1971), p. 339; S. Kida, J. Phys. Jpn. **50**, 3517 (1981); D. G. Dritchel, J. Fluid Mech. **210**, 223 (1990).
[16] C. F. Driscoll, J. H. Malmberg, and K. S. Fine, Phys. Rev. Lett. **60**, 1290 (1988).
[17] A. J. Peurrung and J. Fajans, Phys. Fluids B **5**, 4295 (1993).
[18] X.-P. Huang, Ph.D thesis, UCSD, 1993.
[19] K. S. Fine, C. F. Driscoll, and A. C. Cass, Bull. Am. Phys. Soc. **39**, 1736 (1994).
[20] D. L. Eggleston, Phys. Plasmas **1**, 3850 (1994).
[21] P. B. Rhines and W. R. Young, J. Fluid Mech. **133**, 133 (1983).
[22] T. B. Mitchell and C. F. Driscoll, Phys. Rev. Lett. **73**, 2196 (1994).